International Journal of Image and Graphics
Vol. 5, No. 3 (2005) 1–35

World Scientific
www.worldscientific.com

DETERMINATION OF MINUTIAE SCORES FOR FINGERPRINT IMAGE APPLICATIONS*

PARTHA BHOWMICK
Computer Science and Technology Department
Bengal Engineering College
Shibpur, Howrah 711103, India
partha@becs.ac.in

ARIJIT BISHNU*, BHARGAB BIKRAM BHATTACHARYA†,
MALAY KUMAR KUNDU‡ and C. A. MURTHY§
Indian Statistical Institute
203 B. T. Road, Kolkata-700108, India
**bishnu_t@isical.ac.in*
†*bhargab@isical.ac.in*
‡*malay@isical.ac.in*
§*murthy@isical.ac.in*

TINKU ACHARYA
Avisere Inc., Tuscon, Arizona, USA
and
Department of Electrical Engineering
Arizona State University, Tempe, AZ, USA
tinku.acharya@cox.net

Received 4 March 2003
Revised 6 June 2003
Accepted 1 November 2003

Many Automatic Fingerprint Identification Systems (AFIS) are based on minutiae matching. Minutiae are the terminations and bifurcations of the ridge lines in a fingerprint image. A gray-scale fingerprint image that has undergone binarization, followed by thinning, in order to extract the minutiae, may contain hundreds of minutiae, all of which are not so vivid and obvious in the original image. Thus, the set of minutiae that are well-defined and more prominent than the rest should be given higher relevance and importance in the process of minutiae matching.

In this work, a gray-scale fingerprint image is first preprocessed to produce a thinned binary image. Next, a method to assign a score value to each of the extracted minutiae is

*This work is funded in part by a grant from Intel Corp., USA (PO #CAC042717000), US patent pending.
†Author for correspondence.

proposed, based on certain topographical properties of a minutia. The score associated to a minutia signifies its robustness and prominence. A minutia with a higher score value should be considered with higher priority in the matching scheme to yield better results. Experimental results on several standard databases have been reported.

Keywords: Automatic Fingerprint Identification Systems (AFIS); biometric authentication; fingerprint matching; minutiae.

1. Introduction

Fingerprints, produced by the ridge and valley patterns on the tip of the fingers, have been used for biometric authentication for quite a long time.[9] Owing to their uniqueness and immutability,[19] coupled with easy acquisition procedure, fingerprints provide the most widely used biometric features till today. In the recent years, apart from criminal identification extensively used by law enforcement agencies, fingerprint verification has become more popular in day-to-day civilian applications, such as access control, financial security, employee identification, verification of firearm purchasers, driver license applicants, etc. In the past, fingerprint verification was performed manually by professional fingerprint experts. However, the manual matching of fingerprints is very tedious, time consuming, and expensive. A fingerprint image database may contain as high as several million records, thereby making the manual fingerprint verification an intractable task. Recently, automatic palmprint verification has also received considerable attention.[30]

In order to ensure a much faster and efficient fingerprint matching process, Automatic Fingerprint Identification Systems (AFIS) have evolved in recent times. Most of them are based on minutiae matching. Minutiae, also called Galton's characteristics,[9] are local discontinuities of ridge lines in a fingerprint pattern. The American National Standards Institute (ANSI) has proposed a minutiae classification based on four classes: *Terminations*, *bifurcations*, *trifurcations* (or *crossovers*), and *undetermined*.[1] In practice, most of the AFIS follow the two-class minutiae classification: Termination and bifurcation, used by the Federal Bureau of Investigation (FBI).[31] Since in a fingerprint image, trifurcation and undetermined minutiae, if present, are very few in number, we have adopted the model used by FBI, and have not considered a trifurcation minutia or an undetermined minutia as a valid minutia. The bifurcation and termination minutiae, located in two small regions of size 40 pixels $\times$ 40 pixels each, of a gray-scale fingerprint image having 500 dpi resolution are shown in Fig. 1. These two regions have been carefully selected from a noise-free portion of an image to have a better understanding of how a bifurcation minutia or a termination minutia looks like in a gray-scale image topography. In many situations, however, the minutiae are located in a noisy area when it becomes difficult to recognize them.

In a fingerprint identification system, the fingerprint image is captured by some inking method or a sensor. The acquired image often contains impure patterns or noise caused by under-inking, over-inking, wrinkles, scars, uneven pressure at

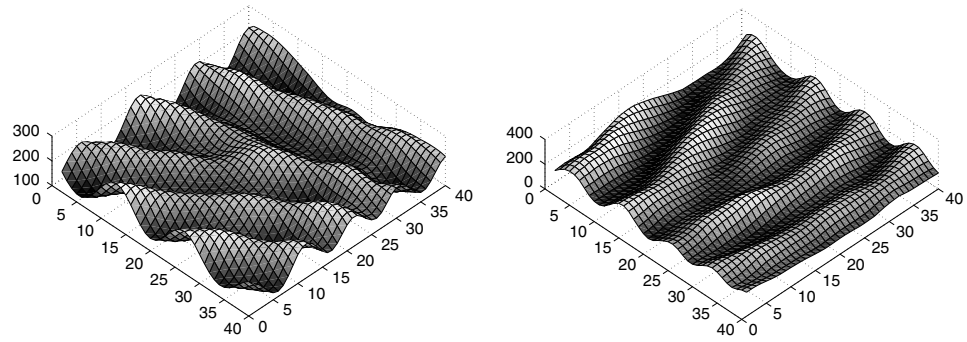

(a) Bifurcation minutia (b) Termination minutia

Fig. 1. Modified view of minutiae depicting gray-scale topography of a fingerprint image.

fingertip, limitations in the digitization system, etc. Extraction of valid minutiae that characterize a fingerprint image is a primary task before starting a matching process. The minutiae extraction can be done either on a gray-scale image[20] or on a binary image.[7,14] Whatever may be the technique of minutiae extraction, the set of extracted minutiae may serve as a distinct feature characterizing the fingerprint image, and can be finally used in the minutiae matching process for fingerprint identification.[7,12,14,17,20,21,25]

Minutiae detection directly from a gray-scale fingerprint image was considered by Maio and Maltoni.[20] The basic idea is to trace the ridge lines on the gray-scale image by "sailing" according to certain directional features. In this scheme, no binarization or thinning is required. Instead, a Gaussian mask for regularizing the uneven "volcano silhouette" of the transverse section of a ridge is used to locate the local maximum corresponding to the ridge center. Computation of local ridge direction is done at every step on each ridge line to traverse successfully along the ridge center line, except when, although very rarely, the ridge has excessive bending. The set of minutiae detected in this approach is then passed through three filters to remove the invalid minutiae, such as low contrast minutiae, pairs of close termination minutiae, and bifurcation minutiae crowded in a small neighborhood.

Both the stages of minutiae extraction and minutiae matching have been described by Jain *et al.*[14] for an online fingerprint verification system. For minutiae extraction, an improved algorithm proposed by Ratha *et al.*[28] is implemented for processing an input gray-scale fingerprint image captured with an online inkless scanner. A new hierarchical method is shown for estimation of local orientation field of flow patterns, followed by a segmentation algorithm to locate the region of interest from the fingerprint image. Binarization is done by convolving the fingerprint image with two masks, adapted to the local ridge width, to accentuate the local maximum gray-level values along the direction normal to the local ridge direction. From the binarized ridge map, the holes and speckles, arising due to the noise present in the input image, are removed before ridge thinning for efficient

minutiae extraction. The thinned ridge map undergoes a smoothing procedure to remove spikes and to join broken ridges. A final refinement, based on the structural informations, is done to eliminate the spurious minutiae, viz., clustered minutiae in a small region, and two close minutiae facing each other. For each surviving minutia, its coordinates, orientation (i.e. local ridge orientation of the associated ridge), and the associated ridge are recorded for matching purpose. The matching procedure consists of two stages, namely, the alignment stage and the matching stage. In the alignment stage, transformations such as translation, rotation and scaling between an input image and a database template are estimated in order to make the input image aligned with the template minutiae according to the estimated parameters (coordinates, orientation, and associated ridge). In the matching stage, both the input minutiae and the template minutiae are converted to polygons in polar coordinate system and an elastic string matching algorithm is used to match the resulting polygons.

In the fingerprint minutiae extraction method developed by Farina *et al.*,[7] a local ridge distance map has been derived from the skeleton image. The local ridge distance map captures the average ridge distance in each region of the image.[18] In this method, the skeleton image is processed pixel by pixel to find the number of outgoing branches that indicate whether or not the candidate pixel is a minutia. This is followed by (i) pre-filtering to delete one minutia from a pair of minutiae lying close to each other, (ii) skeleton enhancement or ridge repair to identify ridge breaks, eliminate bridges, spurs and short ridges, and finally, (iii) removal of islands and validation of bifurcations and end-points. The final valid set of minutiae is classified as either "highly reliable" or "less reliable".

He *et al.*[11] has developed a fingerprint image enhancement and minutiae matching algorithm that is a modification over the method used by Jain *et al.*[14] The method developed by He *et al.* is divided into two phases, off-line and on-line. In the off-line phase, a fingerprint image is acquired, enhanced using orientation fields of ridge directions. Thereafter, features of the fingerprint in terms of minutiae coordinates, its orientation, relation of the minutiae to some points on the associated ridge are extracted and stored in a database as a template. In the next on-line phase, a fingerprint is acquired, enhanced and the same features of the fingerprint are extracted, fed to a matching model and matched against template models in the database. The matching phase is akin to Jain *et al.*'s method,[14] except for three aspects. The difference is in the method of alignment, use of ridge information in the matching process, and the use of a variable bounding box that is more robust to nonlinear deformations between two fingerprints.

Another approach to speed up fingerprint identification problem is the use of indexing. An indexing algorithm, based on the features of triangles formed by the triplets of minutiae, and its performance on two different data sets in a black-box approach have been reported by Bhanu and Tan.[2] The triangle features that are used are its angles, handedness, type, direction, and maximum side. Experimental results on live-scan fingerprint images of varying quality and NIST special database

4 show that the indexing approach efficiently narrows down the number of candidate images in the presence of translation, rotation, scale, shear, occlusion, and clutter. Thus, the indexing technique significantly reduces the number of hypotheses to be considered for the verification algorithm. In other words, in a complete fingerprint recognition system, an indexing technique can be used as front-end processing, which would be then followed by a back-end verification processing.

Apart from minutiae-based fingerprint matching, there exist other matching algorithms that largely depend on the ridge and valley topography of a fingerprint image. Traditional minutiae-based methods suffer from the following shortcomings: (i) they do not fully utilize a significant component of the rich discriminatory information available in the ridge and valley structure of fingerprints; and (ii) they fail to match quickly two fingerprint images containing different number of unregistered minutiae points.[15] In a procedure by Jain *et al.*,[15] a bank of Gabor filters is used to capture both local and global details in a fingerprint as a compact fixed length FingerCode. This scheme tessellates an image to extract its FingerCode, which is the ordered enumeration of the local features contained in the tessellated sectors; the Euclidean distance between two FingerCodes is used for matching. This has been designed with an objective of computationally attractive matching and indexing. In the matching scheme, the concept of scores in the form of vectors is used to express the degree of matching between two fingerprints. Similarly, in the work by Willis and Myers,[32] the total image, or a better representation thereof, is used for the recognition of low-quality fingerprints. After necessary smoothening and enhancing of imperfect images by a threshold FFT technique, valid minutiae are detected to find a reference point by computing a weighted centroid of all valid minutiae and ridge pixels. The reference point is used for a wedge ring overlay minutia detector, and finally, a number of statistical and neural network classifiers are tested to classify the relevant feature vectors for the recognition task. Ceguerra and Koprinska[6] have developed another approach that also combines local as well as global features of a fingerprint image by integrating minutiae and shape signatures that are used in a neural network for final recognition.

2. Preliminaries

A fingerprint image essentially consists of a set of minutiae on the x-y plane. Minutiae are the terminations and bifurcations of ridge lines in a fingerprint image. The ridge lines, appearing in the foreground of the gray-scale topography, are separated by valley lines appearing in the background. In a fingerprint image, there exists a striking duality in the sense that the valley lines also have minutiae (terminations and bifurcations) and flow patterns similar to the ridge lines.[12,13] The ridge and valley characteristics, such as ridge and valley flow directions, inter-ridge and inter-valley distances, ridge and valley breaks, etc., are very useful properties that indicate the validity criteria of a minutia detected by any algorithm. These parameters have been used extensively in a number of earlier works. For enhancing a

gray-level fingerprint image, orientation of ridges is used for designing a filter by O'Gorman and Nickerson,[24] and, for using directional images by Mehtre *et al.*[22] In a work by Hung,[13] ridge enhancement is done based on ridge directions, and noise removal and pattern purification are performed with the help of both ridge and valley characteristics.

A gray-scale fingerprint image often undergoes binarization, followed by thinning, in the preprocessing stage, in order to extract the minutia points.[7,14] In the process of binarization and thinning, several ridge deformations, such as spurs, bridges, short ridges, loops, ridge breaks, become prominent that give rise to false minutiae. These undesired spurious elements in the ridge skeleton owe their origin to the noise present in the original gray-scale image. A spur originating from a point P on a ridge gives rise to a false minutia at P. Among the three branches incident at P, only two branches are aligned while the direction of the third branch that corresponds to a spur is generally different. Moreover, the length of a branch, if forming a spur at P, is within some specified magnitude that helps to identify it as a spur.[7,13] In general, if λ is the local inter-ridge distance of the corresponding minutia, then the length of a spur is not more than $3\lambda/2$. A small region of a gray-scale fingerprint image with 500 dpi resolution that gives rise to a spur is shown in Fig. 2(a), and the corresponding skeletonized version in Fig. 2(b). It is evident from Fig. 2(b) that the spur length is 6 pixels, which is about $\lambda/2$ for the associated block of region. The spur has given rise to two false minutiae: One being a false bifurcation minutia on the ridge from where it has originated, and the other being a false termination minutia where it ends. The two false minutiae arising out of the spur, are shown as black pixels in Fig. 2(b).

Another small region of a gray-scale image topography that contains a bridge and the corresponding skeletonized image are shown in Figs. 3(a) and 3(b). The latter is basically a ternary image, where, the darker lines are ridges and the fainter ones are valleys against a white background. The use of ternary image (ridge, valley, and background) can be found in many existing techniques on fingerprint

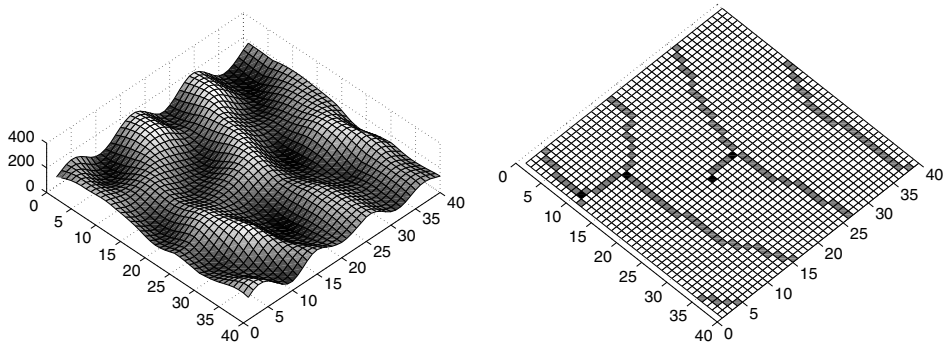

(a) Gray-scale (b) Binary and skeletonized

Fig. 2. Magnified view of spur in a fingerprint image.

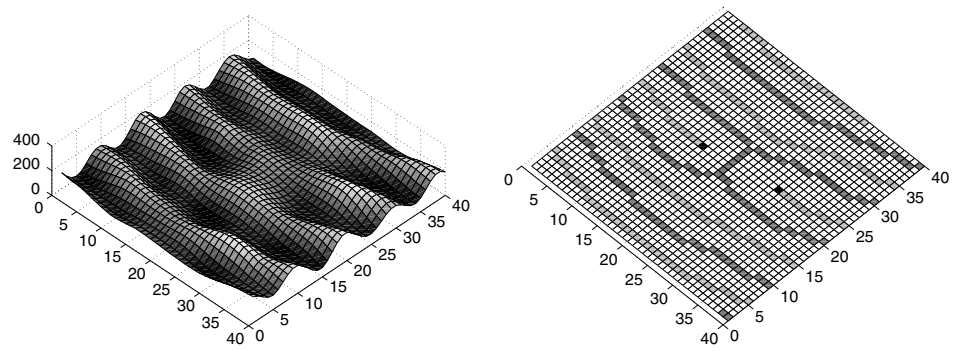

(a) Gray-scale (b) Ternary and skeletonized

Fig. 3. Magnified view of bridge in a fingerprint image.

matching.[3,10,13] A bridge is nearly orthogonal to the pair of ridges it is connected to, and its length is, in general, not more than $3\lambda/2$.[7] Moreover, a bridge gives rise to a valley break,[13] thereby creating two valley terminations on its two sides. The two valley terminations on two sides of the bridge (of ridge skeleton) are shown as black pixels in Fig. 3(b). The bridge itself gives rise to two false minutiae on the pair of ridges it is connected to. Similarly, short ridges, loops, and ridge breaks are also very common image impurities, giving rise to false minutiae, whose characteristic nature and invalidation techniques can be found in the literature.[7,13]

During preprocessing, apart from spurs, bridges, loops, etc., several spurious and misleading lines appear in the thinned image because of the noise present in the original gray-scale image. These lines are mere aberrations that often give rise to poor or not-so-obvious minutiae, thereby delaying the process of minutiae matching, or reporting a poor fingerprint match. Spurs, bridges, loops, etc. are easily detectable in a less noisy region. In a substantially large noisy part of an image, several crisscrosses may arise that are not always detectable as spurs, bridges or loops. A small region from such a noise-affected area is shown in Fig. 4. There may also exist some minutiae in a noise-free region (apparently, by the naked eye) that are feebly recognizable in the gray-scale image because of erratic gray-value pattern in that locality. As a result, an ambiguity may arise regarding the inclusion or exclusion of a minutia depending on its visual clarity in the original gray-scale image.

The postprocessing job on authentication of the detected set of minutiae is also performed in the grayscale domain under supervised learning. The minutiae-based matching procedure by Prabhakar *et al.*[26] uses feedforward of original fingerprint image to the feature (minutiae) verification stage. The image is first normalized and then its contrast is enhanced by appropriate Gabor filters. The verification stage is based on re-examining the grayscale profile in a minutia's spatial neighborhood. The verification stage first learns the characteristics of the ground-truth minutiae and non-minutia regions in the grayscale image in the training phase, which is then used to verify each detected minutia. This stage is based on supervised learning

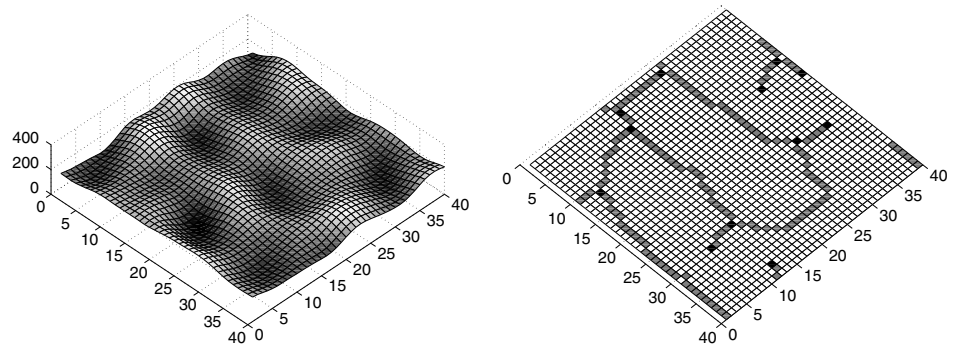

(a) Gray-scale (b) Binary and skeletonized

Fig. 4. Gray-scale topography of a noisy zone and its corresponding skeletonized binary structure.

using Learning Vector Quantization. Here, quality index of an image is measured by an algorithm based on grayscale variance and consistency of ridge orientations to determine regions of good quality, and an overall quality score is assigned to an image, but not to any individual minutia. On the contrary, in our work, we have devised a method to assign scores to all valid minutiae that can be exploited to evaluate the overall quality of the concerned image by an efficient technique. Further, it does not need any training. Prabhakar *et al.*[26] observed that the fingerprint verification system can be improved by a feedforward of the original grayscale image to a feature verification stage. The method however, requires (i) exploring an intelligent scheme for applying the algorithm to only selected locations for minutiae detection, and (ii) devising an efficient training mechanism. Another assertion from their paper that reinforces our findings is that they have mentioned about the possibility of improving the accuracy of the fingerprint verification system by some modified matching algorithm that can take the confidence value (referred to as *score* in our work) of the individual minutiae into account. Another technique proposed by Jiang and Ser[16] improves the fingerprint templates by merging and averaging minutiae of multiple fingerprints. The weighted averaging scheme enables the template to change gradually with time according to the change of skin and imaging conditions. This reduces the storage and computation requirements by its inherent recursive nature. It can be said that our work just echoes the same idea when only one fingerprint image is available for an individual being. In fact, the method of assigning scores to the minutiae will be be of greater significance when we have a series of fingeprint images for the same being over a prolonged period of time.

Main Results

In order to circumvent the aforesaid uncertainty, we propose in this paper, a methodology of assigning a score value to each minutia, after elimination of spurs,

bridges, loops, etc. Each minutia is assigned an integer score in the scale [1, 100] depending on its topographical characteristics in the skeletonized ternary image (ridge, valley, and background), which in turn, are derived from its visual prominence in the original gray-scale image. It may be noted that the proposed score-based technique can be used to expedite both the fingerprint identification problem (1-to-N) and the verification problem (1-to-1).

3. Score-Based Fingerprint Matching

Let A be the set of minutiae, called the *data set*, existing in the fingerprint database, and B be the *query set* of minutiae that has to be checked for a match with some subset of A. The existing matching schemes do not discriminate among the minutiae apropos their quality either in the data set or in the query set. In these schemes, a match is reported if the coordinates, types and angles of minutiae of query set B are found to be agreeing with those of data set A under certain transformations like translation, rotation, or scaling.[12,14,17,20,25] The authenticity of the minutiae is, in general, not taken into consideration.

In order to consider the relative quality of a minutia in a fingerprint image as a practical matching criterion, we define a minutia point P as a 5-tuple, $P = \langle x, y, t, \theta, s\rangle$, where, $\langle x, y\rangle$ = coordinates of P, t = type of minutia (bifurcation or termination), θ = angle made by the tangent to the corresponding ridge at the point P, and s = an integer score associated with the minutia P. The angle θ corresponding to a bifurcation minutia and a termination minutia are shown in Figs. 5(a) and 5(b) respectively. For each valid minutia P, the corresponding value of the associated ridge direction θ can be estimated by the conventional linear regression technique.

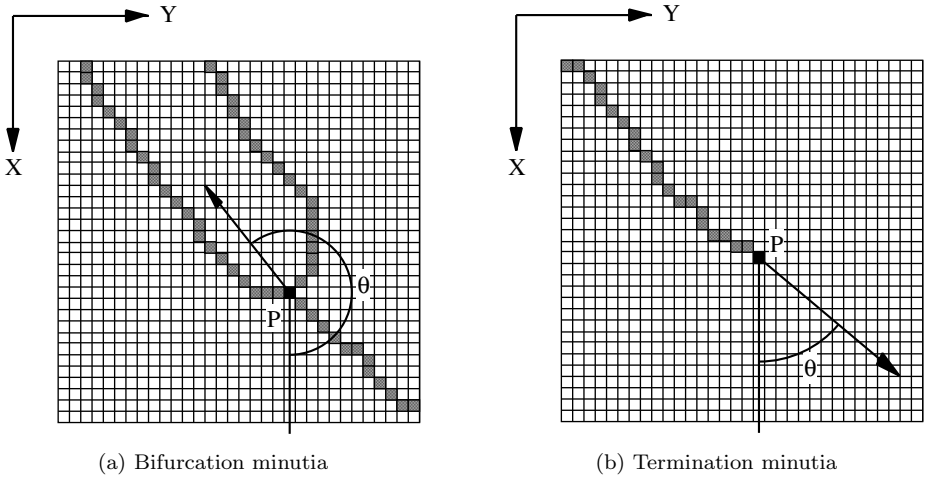

(a) Bifurcation minutia (b) Termination minutia

Fig. 5. Ridge direction θ for a minutia P.

The score values are normalized within a scale of 1 to 100, where, a minutia with score nearing 100 is of the highest significance compared to any other minutia with a lower score value. In other words, if a minutia P_1 has a score s_1, and another minutia P_2 has a score s_2, where $s_1 < s_2$, then P_1 is a less dependable minutia than P_2. Figure 6(a) exhibits a small region of a ternary skeletonized image (ridge, valley, and background) which is free of noise, and Fig. 6(b) shows a similar region affected by noise. It is quite evident from this figure that the minutiae P in Fig. 6(a) will have a fairly high score, whereas, the minutiae P in Fig. 6(b) will have a poor score value. The ridge lines as well as the valley lines in the neighborhood of P in Fig. 6(b) have erratic and irregular flow patterns that indicate the presence of noise in this region. On the contrary, the ridge and valley lines in Fig. 6(a) show a smooth flow pattern that speaks of the tidiness of the region. In Figs. 6(a) and 6(b), the darker (fainter) lines represent the ridges (valleys). Both the ridge minutiae and valley minutiae in these figures are highlighted by black pixels.

While applying a fingerprint matching procedure based on minutiae, the scores of minutiae of A and those of B can be used to predict how good or bad the match is. Let A' be a subset of A, and B' be a subset of $B^{R,T,S}$, where, $B^{R,T,S}$ has been obtained from B after suitable transformations of rotation (R), translation (T), and scaling (S), such that A' and B' form the best possible matching pair of subsets. Let $|A| = n_a$, $|B| = n_b$, and $|A'| = |B'| = n_{match}$. If a minutia (x_{a_i}, y_{a_i}) with score s_{a_i} in set A' is a potential match with a minutia (x_{b_i}, y_{b_i}) with score s_{b_i} in set B', the difference between s_{a_i} and s_{b_i} ($s_{a_i} \sim s_{b_i}$) indicates the quality of matching of (x_{a_i}, y_{a_i}) and (x_{b_i}, y_{b_i}). For a matching between A and B with n_{match} minutiae, we

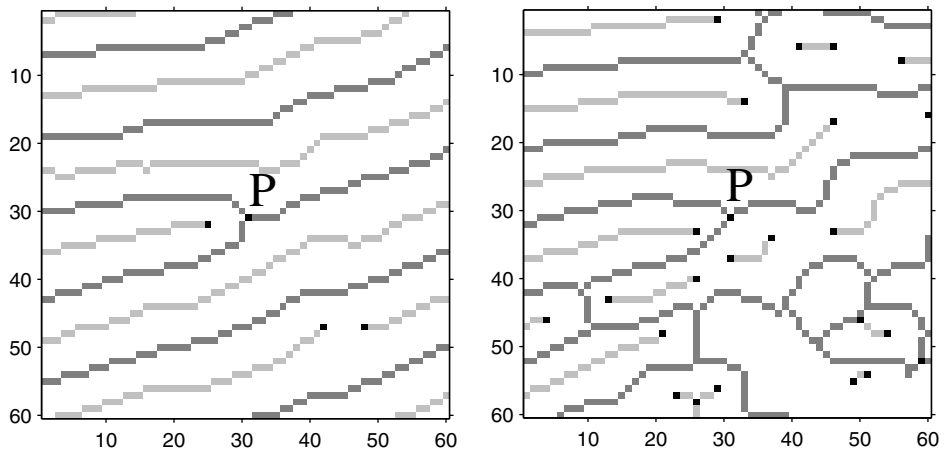

(a) Minutia P with high score (b) Minutia P with low score

Fig. 6. Typical ridge and valley skeletons in the local neighborhood of a strong minutia (with high score) and a weak minutia (with low score).

define the *matching index* MI as follows:

$$MI = \frac{1}{n_{max}} \sum_{i=1}^{n_{match}} \left\{ \frac{1}{2}(s_{a_i} + s_{b_i}) - \omega |s_{a_i} - s_{b_i}| \right\}, \quad (1)$$

where, $n_{max} = max(n_a, n_b)$, and $0 \leq \omega \leq \frac{101}{198}$.

The rationale behind Eq. (1) is as follows. Since $1 \leq s_{a_i}, s_{b_i} \leq 100$ for $1 \leq i \leq n_{match}$, the maximum value of $(s_{a_i} + s_{b_i})$ is 200, whereas, the minimum value is 2. Thus, for a match between two best possible minutiae, each with score 100, a value of 100 is contributed to the matching index. Similarly, a value of 1 is contributed due to a match between two worst possible minutiae, each with score 1. The parameter ω represents the weightage attached to the difference of scores of two matching minutiae in their way of participating in the estimate of MI. It can be shown that the value of ω should lie between 0 and $\frac{101}{198}$ so that $\left\{\frac{1}{2}(s_{a_i} + s_{b_i}) - \omega |s_{a_i} - s_{b_i}|\right\}$ is never negative. The case of worst matching (hence a minimum contribution to MI in Eq. (1)) between two corresponding minutiae arises when, without loss of generality, $s_{a_i} = 100$ and $s_{b_i} = 1$, that is, s_{a_i} and s_{b_i} differ by maximum extent. Therefore, in order to reduce the contribution to MI for the worst case to as low as zero (the lowest possible in our procedure), we should have, as per Eq. (1), $\frac{1}{2}(100+1) - \omega|100-1| = 0, or, \omega = \frac{101}{198}$. A high value of ω nearing $\frac{101}{198}$ signifies that not only the average score of the matching minutiae is considered in the estimate of MI, but their difference in scores is also taken into consideration with a high weightage. For instance, for $\omega = \frac{1}{2}$, if $s_{a_i} > s_{b_i}$, then the contribution to MI by the corresponding match is $\frac{1}{2}(s_{a_i} + s_{b_i}) - \frac{1}{2}(s_{a_i} - s_{b_i}) = s_{b_i} = min(s_{a_i}, s_{b_i})$. Similarly, for $\omega = \frac{1}{2}$, if $s_{b_i} > s_{a_i}$, then the contribution to MI by the corresponding match is $\frac{1}{2}(s_{a_i} + s_{b_i}) - \frac{1}{2}(s_{b_i} - s_{a_i}) = s_{a_i} = min(s_{a_i}, s_{b_i})$. Thus, for $\omega = \frac{1}{2}$, if one of s_{a_i} and s_{b_i} is very high, and the other one very low, the contribution to MI by the matching pair (x_{a_i}, y_{a_i}) and (x_{b_i}, y_{b_i}) is as poor as the score of the minutia of worse quality. However, as ω approaches 0, the contribution to MI by the matching pair (x_{a_i}, y_{a_i}) and (x_{b_i}, y_{b_i}) approaches the average score of this minutiae pair.

Furthermore, from Eq. (1), it is also evident that if n_{match} is quite small compared to n_{max}, MI will be also quite low even though the scores of all matching minutiae may be very high. Similarly, MI will also be quite low if scores of each pair of matching minutiae vary widely instead of n_{match} being close to n_{max}. MI will be high only if n_{match} is close to n_{max} and all matching minutiae are of good quality. The ideal case for $MI = 100$ occurs only when $n_a = n_b = n_{match}$ and $s_{a_i} = s_{b_i} = 100$, for $i = 1, 2, \ldots, n_{match}$. A score-based generic structure of an AFIS is shown in Fig. 7.

4. Evaluation of score

The score s of a minutia P is estimated based on the following properties:

- pattern of ridge flow in and around P

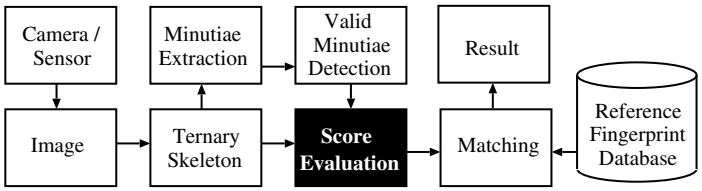

Fig. 7. Generic structure of an AFIS considering minutiae scores.

- pattern of valley flow in and around P
- noise level in the locality of P.

If the ridge and valley lines in the local neighborhood of P have a smooth nature of flow, the corresponding minutia P will have a genuine contribution in the fingerprint matching. On the contrary, if in some region, the ridge and valley lines have an erratic or uneven nature of flow, a minutia P' in that region should not predominate the matching procedure. The former minutia (P), being located in a tidy region, lends more confidence in the matching procedure than the latter (P'), which is located in a noisy region.

For a minutia $P(x, y)$, the score is given by the equation

$$s = \lfloor s_{ri} \rfloor + \lfloor s_{va} \rfloor + \lfloor s_{no} \rfloor, \tag{2}$$

where, s_{ri}, s_{va} and s_{no} are the score components due to ridge flow, valley flow, and noise level respectively in the local neighborhood of P. The components s_{ri} and s_{va} denote measures of perfectness of ridge and valley flow respectively, that are evaluated based on some distances estimated in the local ridge and valley topography around the minutia P. To take into account the noise of the region in and around P, the component s_{no} is estimated in a local window centered at P. Noise imparts a negative effect on the score.

4.1. *Score of a bifurcation minutia*

Let λ be the average inter-ridge distance of a fingerprint image. First, we find the three neighbor pixels N_1, N_2, N_3 of P, considering 8-neighborhood. N_1, N_2, N_3 are the three starting pixels of the ridges r_1, r_2, r_3 respectively, incident at P. We explore a walk along each of r_1, r_2, r_3 starting from N_1, N_2, N_3 respectively, each walk being of length λ. Let these walks be named as w_1, w_2, and w_3 respectively. If during some walk w_i, $1 \leq i \leq 3$, any bifurcation or termination minutia is encountered, the walk is halted. Let, l_i, $1 \leq i \leq 3$, denote the length of the walk w_i. Let, l_{min} be the minimum of l_i, $1 \leq i \leq 3$, and μ be the number of walks whose lengths are less than λ. If P is a minutia of good quality, then each l_i should be at least $\lambda/2$, and at least two of them should be λ. So, if $l_{min} < \lambda/2$ or, $\mu \geq 2$, we assign 0 to *score* and return from this point. Otherwise, if $l_{min} < \lambda$, then we walk for a length l_{min} along each of the three ridges r_1, r_2, r_3 starting from N_1, N_2, N_3

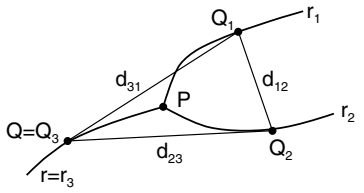

Fig. 8. Ridges r_1, r_2, and r_3 incident at the bifurcation minutia P.

respectively, so that after the (re-)walks, each of the points Q_1, Q_2, Q_3, reached on the three ridges r_1, r_2, r_3 respectively, is at equal distance from P (Fig. 8).

In this scenario, we need to identify the ridge line that bifurcates at P. In Fig. 8, the three ridges are shown as r_1, r_2, and r, where r $(=r_3)$ has been depicted as the pre-bifurcated ridge, and r_1, r_2 are its two bifurcations at P. To identify the pre-bifurcated ridge, we define $d_{min} = min(d_{12}, d_{23}, d_{31})$, where, $d_{ij} = L_2$-distance between $Q_i(x_i, y_i)$ and $Q_j(x_j, y_j) = [(x_i - x_j)^2 + (y_i - y_j)^2]^{\frac{1}{2}}$, $1 \leq i, j \leq 3$, $i \neq j$. If Q_1 and Q_2 are on the two bifurcated ridges r_1 and r_2, then $d_{12} < d_{23}$ and $d_{12} < d_{31}$. However, this condition may fail if P is a poor minutia candidate, viz., when the ridges incident at P are of uneven nature, and it is difficult to ascertain the pre-bifurcated ridge among r_1, r_2, r_3. Hence, if $d_{min} > 3l_{min}/2$, we assign 0 to *score*, and return.

In order to compute the score s_{ri} for a bifurcation minutia P, we define the following distances, vide Fig. 9.

d_{qn_1}= distance from Q to neighbor ridge $n_1 = QK_1$
d_{qn_2}= distance from Q to neighbor ridge $n_2 = QK_2$
$d_{q_1n_1}$= distance from Q_1 to neighbor ridge $n_1 = Q_1M_1$
$d_{q_2n_2}$= distance from Q_2 to neighbor ridge $n_2 = Q_2M_2$

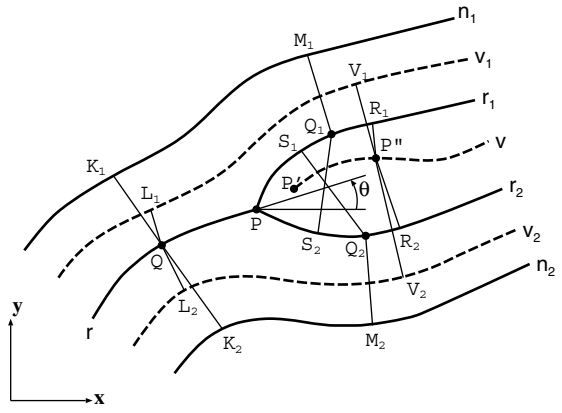

Fig. 9. Ridge and valley characteristics in the local neighborhood of a bifurcation minutia.

$d_{q_1r_2}$= distance from Q_1 to bifurcated ridge $r_2 = Q_1S_2$
$d_{q_2r_1}$= distance from Q_2 to bifurcated ridge $r_1 = Q_2S_1$.

For a good minutia, the above distances should be close to λ. So, s_{ri} is assigned to P depending on the closeness of $d_{BM,ri} \in \{d_{qn_1}, d_{qn2}, d_{q_1n_1}, d_{q_2n_2}, d_{q_1r_2}, d_{q_2r_1}\}$ w.r.t. λ. Thus, for a bifurcation minutia P, the score w.r.t. the ridge characteristics can be chosen as:

$$s_{ri} = \alpha_{ri} \sum_{d_{BM,ri}} \frac{1}{\lambda}(\lambda - |\lambda - d_{BM,ri}|), \tag{3}$$

where α_{ri} is the ridge score multiplier for bifurcation minutiae.

Similarly, the score s_{va} for the bifurcation minutia P is based on the following set of distances:

d_{qv_1}= distance from Q to neighbor valley $v_1 = QL_1$
d_{qv_2}= distance from Q to neighbor valley $v_2 = QL_2$
$d_{pp'}$= distance from P to valley termination minutia P', if any, lying near P in between r_1 and $r_2 = PP'$
$d_{p''r_1}$= distance from P'' to bifurcated ridge $r_1 = P''R_1$
$d_{p''r_2}$= distance from P'' to bifurcated ridge $r_2 = P''R_2$
$d_{p''v_1}$= distance from P'' to neighbor valley $v_1 = P''V_1$
$d_{p''v_2}$= distance from P'' to neighbor valley $v_2 = P''V_2$,

where, P'' is the point along the valley v at a distance λ from P', or, a bifurcation or termination of v appearing within the target walk-length of λ. The distances $d_{pp'}$, $d_{p''r_1}$, $d_{p''r_2}$, $d_{p''v_1}$, and $d_{p''v_2}$ exist only if P' exist near P in between r_1 and r_2. Angle θ, the local ridge direction of r at P, serves as the guiding vector to search for such a P', as shown in Fig. 10, as follows.

Consider the vector $\overrightarrow{PX_\theta}$ from the minutia P at an angle θ w.r.t. $(+)x$-axis. Let $D_1, D_2, D_3, \ldots$ be the points on $\overrightarrow{PX_\theta}$ at distances of 1 unit, 2 units, 3 units, ..., respectively, from P. The search for finding a valley termination operates in an iterative way for a maximum number of $\frac{3\lambda}{2}$ steps. In the ith step, we consider the

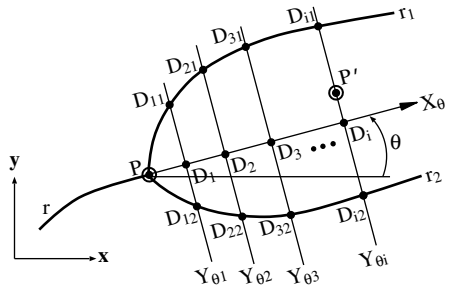

Fig. 10. Searching for the valley termination minutia P' along the tangent vector PX_θ corresponding to the ridge bifurcation minutia P.

line $\overleftrightarrow{D_i Y_{\theta i}}$ passing through D_i and perpendicular to $\overrightarrow{PX_\theta}$. Let D_{i1} and D_{i2} be the points at which $\overleftrightarrow{D_i Y_{\theta i}}$ intersects the two bifurcated ridges, r_1 and r_2. At each point on the line segment $\overline{D_{i1}D_{i2}}$, we check whether it is valley minutia. If the point is a valley minutia (P'), the search terminates.

While the parameter $\{d_{BM,ri}\}$ represents some kind of inter-ridge distance, we define other distance measures with a subtle difference. Distances in the set $\{d^1_{BM,va}\} = \{d_{p''v_1}, d_{p''v_2}\}$ are inter-valley distances, which should be ideally close to λ. The other set $\{d^2_{BM,va}\} = \{d_{qv_1}, d_{qv_2}, d_{pp'}, d_{p''r_1}, d_{p''r_2}\}$ contains distances from a ridge point to a valley line, or from a valley point to a ridge line, and therefore, allowed for a flexibility in their contribution to s_{va}. Hence, distances in the set $\{d^1_{BM,va}\}$ are very much similar to $\{d_{BM,ri}\}$ as far as the estimation of s_{va} is concerned. Their contribution to score may be chosen as:

$$s^1_{va} = \alpha_{va} \sum_{d^1_{BM,va}} \frac{1}{\lambda}\big(\lambda - \big|\lambda - d^1_{BM,va}\big|\big). \tag{4}$$

And, that due to $\{d^2_{BM,va}\}$ is

$$s^2_{va} = \sum_{d^2_{BM,va}} s_{d^2_{BM,va}}, \tag{5}$$

where, $s_{d^2_{BM,va}}$ is chosen as:

$$s_{d^2_{BM,va}} = \begin{cases} \alpha_{va} \cdot 1 & \text{if } \lambda/4 \le d^2_{BM,va} \le 3\lambda/4 \\ \alpha_{va}\ \frac{1}{\lambda}\big(d^2_{BM,va} - \lambda/4\big) & \text{if } d^2_{BM,va} < \lambda/4 \\ \alpha_{va}\ \frac{1}{\lambda}\big(3\lambda/4 - d^2_{BM,va}\big) & \text{if } d^2_{BM,va} > 3\lambda/4 \end{cases}, \tag{6}$$

and α_{va} is the valley score multiplier for a bifurcation minutia.

A brief reasoning for the development of Eq. (6) is as follows. Since $d^2_{BM,va}$ is the distance from a ridge point to a neighboring valley line, or from a valley point to a neighboring ridge line, it should be ideally equal to $\lambda/2$. But by allowing a tolerance of $\pm\lambda/4$, a contribution of α_{va} to the score is made if $d^2_{BM,va}$ lies within $\lambda/4$ and $3\lambda/4$. On the other hand, the contribution to score is made negative if $d^2_{BM,va}$ is not within the desired bounds. Furthermore, to incorporate the deviation of $d^2_{BM,va}$ from the desired value, the contribution by $d^2_{BM,va}$ is made more and more negative as it goes farther and farther from $\lambda/4$ or $3\lambda/4$.

4.2. *Score of a termination minutia*

Let P be a termination minutia and N be the adjacent ridge pixel of P, considering 8-neighborhood. Since P is a termination minutia, there will be only one ridge line, say r, incident at P (Fig. 11). We walk along r starting from N, for a length λ, and designate the walk as w. Let l denote the length of the walk. Since a skeletonized fingerprint image should be devoid of spurs and bridges, l should always be equal to λ.

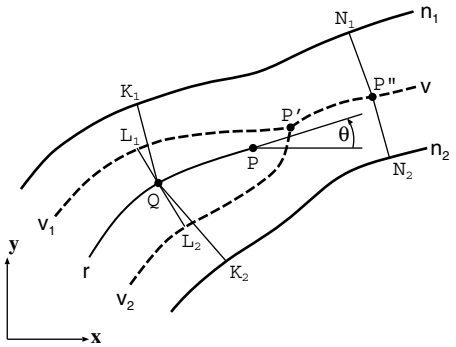

Fig. 11. Ridge and valley characteristics in the local neighborhood of a termination minutia P.

Let Q be the point on the ridge r reached after the walk w. For estimation of the score s_{ri} for the termination minutia with respect to ridge lines in the region containing P, we define the set $\{d_{TM,ri}\}$ of the following distances:

d_{qn_1}= distance from Q to neighbor ridge $n_1 = QK_1$
d_{qn_2}= distance from Q to neighbor ridge $n_2 = QK_2$.

For P to be a termination minutia of good quality, the above distances, should be close to λ. These distances are basically inter-ridge distances similar to $\{d_{BM,ri}\}$ in the case of bifurcation minutiae. Hence, the score s_{ri} is assigned to P based on the following equation that resembles with Eq. (3) in the form:

$$s_{ri} = \beta_{ri} \sum_{d_{TM,ri}} \frac{1}{\lambda}(\lambda - |\lambda - d_{TM,ri}|); \tag{7}$$

where, β_{ri} is the ridge score multiplier for termination minutiae.

Similarly, the score s_{va} for the termination minutia P is based on the set $\{d_{TM,va}\}$ of following distances:

d_{qv_1}= distance from Q to neighbor valley $v_1 = QL_1$
d_{qv_2}= distance from Q to neighbor valley $v_2 = QL_2$
$d_{pp'}$= distance from P to valley termination minutia P', if any, lying near P in between n_1 and $n_2 = PP'$
$d_{p''n_1}$= distance from P'' to neighbor ridge $n_1 = P''N_1$
$d_{p''n_2}$= distance from P'' to neighbor ridge $n_2 = P''N_2$,

where P'' is the point along the valley v at a distance λ from P', or, a bifurcation or termination of v appearing within the target walk-length of λ. The distances $d_{pp'}$, $d_{p''n_1}$, and $d_{p''n_2}$ exist only if P' is found near P in between n_1 and n_2. Angle θ, the local ridge direction of r at P, serves as the guiding vector to search for P'. The procedure of searching for such a valley minutia P' is very much similar to that discussed in Sec. 4.1.

The above set of distances are measured either from a ridge point to a valley line or from a valley point to a ridge line. Hence, their contribution to score s_{va} is given by:

$$s_{va} = \sum_{d_{TM,va}} s_{d_{TM,va}}, \tag{8}$$

where, $s_{d_{TM,va}}$ is chosen as:

$$s_{d_{TM,va}} = \begin{cases} \beta_{va} \cdot 1 & \text{if } \lambda/4 \le d_{TM,va} \le 3\lambda/4 \\ \beta_{va}\ \frac{1}{\lambda}(d_{TM,va} - \lambda/4) & \text{if } d_{TM,va} < \lambda/4 \\ \beta_{va}\ \frac{1}{\lambda}(3\lambda/4 - d_{TM,va}) & \text{if } d_{TM,va} > 3\lambda/4 \end{cases}, \tag{9}$$

and β_{va} is the valley score multiplier for a termination minutia.

The rationale behind Eq. (9) is the same as that for Eq. (6).

4.3. *Estimation of noise*

Let P be a bifurcation or termination minutia having a positive score after the evaluation of s_{ri} and s_{va}. If P does not have a positive score, we need not evaluate s_{no}, since s_{no} will contribute a negative score to P; finally we will consider only the set of minutiae with postive scores. Consider a circular window W of radius $R = N\lambda$ centered around $P(x, y)$, vide Figs. 12 and 13. In Fig. 12, W lies entirely within the region of interest (ROI), whereas, in Fig. 13, W has a partial overlap with the region of interest (ROI) of the corresponding image. Let W' be the region of overlap between W and ROI of the image. Let $\{Q_i | Q_i \text{ lies within } W'; i = 1, 2, \ldots, \eta\}$ be the set of points, with each point Q_i satisfying any one of the following 3 properties (Figs. 12 and 13):

(i) Q_i is a ridge minutia with $s_{ri} + s_{va} \le 0$
(ii) Q_i is a non-minutia ridge point having three or more ridges incident upon it
(iii) Q_i is either a valley bifurcation or a valley termination minutia.

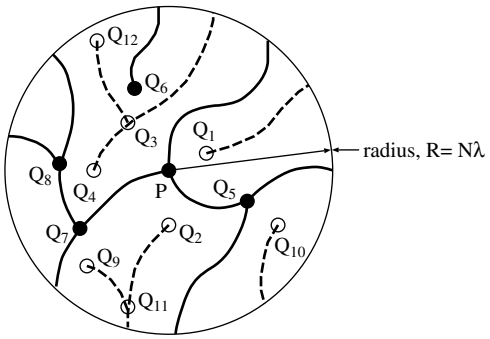

Fig. 12. Example showing contributing points $\{Q_1, Q_2, \ldots, Q_{12}\}$ in a circular window W centered around the minutia P. The window W lies entirely within the region of interest.

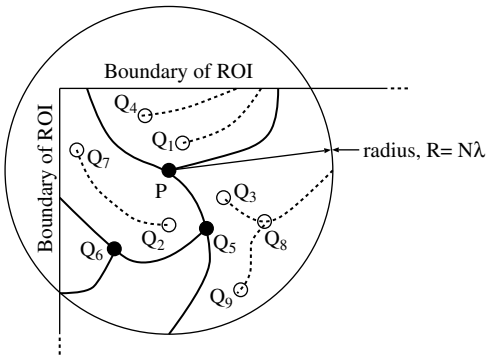

Fig. 13. Contributing points $\{Q_1, Q_2, \ldots, Q_9\}$ in a noisy window W centered around the minutia P. The window W has partial overlap with the region of interest.

The above definition enables us to use $|\{Q_i\}| = \eta$ as a measure of noise level in the window W centered around P. We define another parameter ν, called the *noise factor*, which is used to find the *noise threshold*, τ_{noise}, given in the equation below, that will indicate whether or not the window W associated with a minutia P is noisy:

$$\tau_{noise} = \nu \frac{A}{\lambda^2}, \tag{10}$$

where A is the net area of overlap between W and the region of interest (ROI) of the image. In Fig. 12, since W is entirely within the ROI, $A = \pi R^2$, whereas, in Fig. 13, since W lies partially within the ROI, A is less than πR^2. The contributing points will be more in number as the overlap between W and ROI is high, and lesser in number when W is centered at a minutia P located near the border of ROI. Hence the factor $\frac{A}{\pi R^2}$ is directly related to the number of contributors within the circular window W. Also, since $R = N\lambda$, the area of window W is directly proportional to N^2 for the concerned image. Hence, on the assumption that the number of contributors within W varies directly with the area of W, Eq. (10) is derived as follows.

$$\tau_{noise} = [\text{constant}] \times N^2 \frac{A}{\pi R^2} = [\text{constant}] \times \frac{A}{\pi \lambda^2} = \nu \frac{A}{\lambda^2}.$$

If η is higher than τ_{noise} in W corresponding to P, the noise level in W is considered high enough and each point Q_i, $i = 1, 2, \ldots, \eta$, is accounted one by one for their individual contribution to the noise-induced (negative) score s_{no} of P. Thus, Eq. (11) can be used to find s_{no}^i attributed by each Q_i, and Eq. (12) sums up the individual scores to compute the total score component due to noise:

$$s_{no}^i = \gamma(R - L_2(P, Q_i)), \tag{11}$$

$$s_{no} = \begin{cases} 0 & \text{if } \eta \le \tau_{noise} \\ \sum_{i=1}^{\eta} s_{no}^i & \text{if } \eta > \tau_{noise} \end{cases}, \tag{12}$$

where, γ is the noise score multiplier.

In Eq. (11), L_2-distance between two points $P(x, y)$ and $Q_i(x_i, y_i)$ is given by:

$$L_2((x, y), (x_i, y_i)) = \sqrt{(x - x_i)^2 + (y - y_i)^2}. \quad (13)$$

4.4. *Normalization of score*

In order to bound the minutiae scores in the range of [1, 100], the value of α_{ri} ($= \alpha_{va}$) has been chosen as $\frac{100}{13}$. The reason is as follows. For evaluating the score of a bifurcation minutia, we need to compute 6 distances in the set $\{d_{BM,ri}\}$, measured w.r.t. different ridge lines, and 7 distances in the set $\{d_{BM,va}\}$, measured w.r.t. different valley lines. In each of the three Eqs. (3), (4) and (6), the value of each of the 13 score elements before getting multiplied by α_{ri} or α_{va} is at most unity. Since there are 13 such score elements, 6 from $\{d_{BM,ri}\}$ and 7 from $\{d_{BM,va}\}$, the maximum score obtainable by a bifurcation minutia, before getting multiplied by the ridge score multiplier and valley score multiplier, is 13. Assigning $\alpha_{ri} = \alpha_{va} = \frac{100}{13}$ fixes the total maximum score to 100. Another suggestive choice can be $\alpha_{ri} = \frac{50}{6}$ and $\alpha_{va} = \frac{50}{7}$, giving equal weightage to the total ridge score component and total valley score component. Our choice for $\alpha_{ri} = \alpha_{va} = \frac{100}{13}$ comes from the principle of assigning equal weightage to all 13 distance measures instead of assigning equal weightage to the two different score components.

Similarly, for finding the score of a termination minutia with respect to the ridge and valley skeletons, we measure 7 distances in total, 2 distances in the set $\{d_{TM,ri}\}$ and 5 in $\{d_{TM,va}\}$, respectively. In choosing the values for β_{ri} and β_{va}, we have adopted to equal weightage for all these 7 distances, rather than equal weightage to total ridge score component and total valley score component. Therefore, in our experiments, we have taken $\beta_{ri} = \beta_{va} = \frac{100}{7}$.

5. Experimental Results

We used the fingerprint images from (i) NIST Special Database 4,[27] (ii) NIST Special Database 14,[5] (iii) Database B1 of FVC2000,[8] and (iv) Database B2 of FVC2000.[8] Our experiments for evaluation of scores have been performed on (i) 50 images of set, (ii) 124 images of set, (iii) 80 images of set, (iv) and 80 images of set. Each image in these four sets is a 8-bit gray-scale image. The images of set (i) are used after applying Wavelet Scalar Quantization implemented in PCASYS.[5] A few of the sample images are shown in Appendix 1.

First, the input image is transformed to a skeletonized ternary image consisting of ridges, valleys, and backgrounds. In order to get the skeletonized ternary image from a gray-scale image, we have used the tool *RIVEX* developed by us.[29] For the detection of minutiae from a skeletonized binary image, consisting of ridges(1) against background(0), or valleys(1) against background(0), we have used another tool named as *MINUBIN*.[23] Four gray-scale images each from set (i), set (ii), set (iii) and set (iv) are shown in Figs. 18, 19, 20, and 21 respectively. The images of set (i) and set (ii) are of size 480×512 each, those of set (iii) are of size 300×300,

and those of set (iv) of size 364×256. All the images in these four sets are recorded at 500 dpi.

The results obtained over the four sets of images are presented in Table 1. In Table 1, column 3 indicates the number of images considered for generating the results shown. Column 5 indicates the average number of minutiae with positive scores, n_k, for kth set, vide Eq. (14). Column 6 gives the overall mean score, μ_k, for the corresponding set of images, estimated from the individual mean scores of all the images in the set, μ_{kj}, in accordance with the Eq. (15).

$$n_k = \frac{1}{m_k} \sum_{j=1}^{m_k} n_{kj}, \tag{14}$$

$$\mu_k = \frac{\sum_{j=1}^{m_k} n_{kj}\, \mu_{kj}}{\sum_{j=1}^{m_k} n_{kj}}, \tag{15}$$

where, m_k = total number of images in kth set, n_{kj} = number of minutiae with positive scores, and μ_{kj} is the mean score over all minutiae with positive scores, in jth image of kth set, $k \in \{\mathrm{i}, \mathrm{ii}, \mathrm{iii}, \mathrm{iv}\}$, as shown in the Eq. (16).

$$\mu_{kj} = \frac{1}{n_{kj}} \sum_{i=1}^{n_{kj}} s_{kji}, \tag{16}$$

where, s_{kji} is the (positive) score of ith minutiae in the jth image of kth set.

In Table 1, column 7 displays the overall standard deviation, σ_k, for the corresponding set of images, vide Eq. (17), estimated from the individual standard deviations, σ_{kj}, of all the images in the set, in accordance with the Eq. (18). Average time for evaluating the scores of all minutiae per image of a database is given in column 8.

$$\sigma_k = \left[\frac{\sum_{j=1}^{m_k} \left(n_{kj}\, \sigma_{kj}^2 + n_{kj}\, \mu_{kj}^2 \right)}{\sum_{j=1}^{m_k} n_{kj}} - \mu_k^2 \right]^{\frac{1}{2}}, \tag{17}$$

$$\sigma_{kj} = \left[\frac{1}{n_{kj}} \sum_{i=1}^{n_{kj}} (s_{kji} - \mu_{kj})^2 \right]^{\frac{1}{2}}. \tag{18}$$

Table 1. Results for 4 sets of images.

Set	Database	No. of Images	Image Size	Avg. no. of Minutiae	Mean Score	Std. dev. Score	Avg. time in sec.
i	NIST sdb-4	50	480×512	33	33.55	22.38	0.121
ii	NIST sdb-14	124	480×512	59	48.92	21.84	0.125
iii	FVC-2000 set-B db-1	80	300×300	16	32.46	19.13	0.045
iv	FVC-2000 set-B db-2	80	364×256	23	36.20	20.51	0.053

In the estimation of noise-based score, a number of parameters are involved. N decides the area covered by the window W. A higher value of N includes the distant contributors responsible for noise, whereas, a lower value often fails to incorporate the real noise contributors. Optimization of N is, therefore, a crucial factor. ν decides the noise threshold τ_{noise} that plays a vital role in deciding the noise level of the window W. The controlling paramater γ decides the influence of noise on the score. A higher value of γ will enforce a higher impact of noise in the score. Table 2 enumerates the roles played by the noise detection parameters. Different sets of

Table 2. Variation of score with different parameters.

Image file	N	ν	γ	n_i	n_f	$\Delta n(\%)$	Mean Score
fpi.001.01	1.0	2.00	0.10	77	51	33.77	60.25
fpi.001.02	1.0	2.00	0.20	77	50	35.06	54.12
fpi.001.03	1.0	1.00	0.10	77	51	33.77	54.06
fpi.001.04	1.0	1.00	0.20	77	50	35.06	39.22
fpi.001.05	2.0	3.00	0.10	77	51	33.77	65.35
fpi.001.06	2.0	3.00	0.20	77	51	33.77	65.35
fpi.001.07	2.0	2.00	0.10	77	46	40.26	65.91
fpi.001.08	2.0	2.00	0.20	77	45	41.56	66.89
fpi.001.09	2.0	1.00	0.10	77	41	46.75	48.24
fpi.001.10	2.0	0.50	0.10	77	41	46.75	38.54
fpi.001.11	2.0	0.50	0.20	77	15	80.52	57.07
fpi.001.12	3.0	1.00	0.10	77	32	58.44	66.72
fpi.001.13	3.0	0.75	0.10	77	19	75.32	58.32
fpi.001.14	3.0	0.50	0.10	77	17	77.92	45.82

Table 3. Score distribution for different images.

No.	Image	Minutiae before Score	Minutiae with (+)ve Scores	Mean Score	Std. Dev. of Scores
1	nist.14.1	77	37	59.70	31.59
2	nist.14.2	79	40	58.67	32.25
3	nist.14.3	82	34	60.71	28.66
4	nist.14.4	111	66	62.12	28.05
5	nist.4.1	97	12	44.42	29.26
6	nist.4.2	95	28	35.50	24.43
7	nist.4.3	144	18	28.83	26.61
8	nist.4.4	111	24	33.88	25.25
9	fvc.b1.1	20	11	51.55	17.25
10	fvc.b1.2	34	19	38.74	21.87
11	fvc.b1.3	39	10	44.10	19.06
12	fvc.b1.4	45	11	24.36	28.33
13	fvc.b2.1	20	16	54.62	26.41
14	fvc.b2.2	13	11	51.68	28.01
15	fvc.b2.3	26	22	55.73	35.07
16	fvc.b2.4	25	14	62.64	28.93

values of these parameters have been chosen carefully to demonstrate their effects on the scores of minutiae for a ternary skeleton image fpi.001 exhibited in Fig. 14. In Table 2, the column with heading n_i indicates the initial number of minutiae that are present in the image fpi.001 (Fig. 14) prior to score evaluation. For each set of parameters, the corresponding final number of minutiae with positive scores is shown in column with heading n_f. The column with heading $\Delta n(\%)$ shows the percentage of difference of n_f from n_i. The images with (positively) scored minutiae for different sets of parameters are shown in Fig. 15(a) to Fig. 15(n). In all of these ternary images shown, the darker lines represent the ridges and the faint lines the valleys.

To show our experimental results on the 4 sets of images, we go for choosing $N = 2.00$, $\nu = 1.25$, $\gamma = 0.10$. The corresponding image for our chosen set of parameters with some score values written beside the corresponding minutiae is shown in Fig. 16, the darkness of a minutia being proportional to its score. Table 4 includes the scores (positive values only) of the bifurcation minutiae (BM), followed by those of the termination minutiae (TM), arranged in ascending orders.

Four typical minutiae out of the 77 minutiae of fpi.001 (Fig. 14) are selected along with their neighborhood regions of size 70×70 pixels, shown in Fig. 17, to clarify the three score components, s_{ri}, s_{va} and s_{no}, of these minutiae. Each of these minutiae are located in the center of their corresponding regions in Fig. 17.

In the minutiae P_1 (type: Bifurcation, x: 345, y: 414), each of the three score components is 0. This is due to the fact that all the three ridges incident at P_1 are less than λ in length, thereby failing to establish a positive ridge score for P_1, vide Sec. 4.1. Furthermore, the three ridges incident at P_1 may be very short

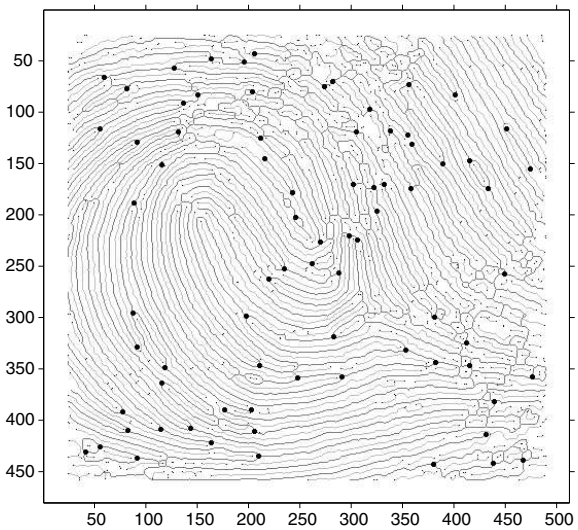

Fig. 14. fpi.001 with 77 minutiae without scores.

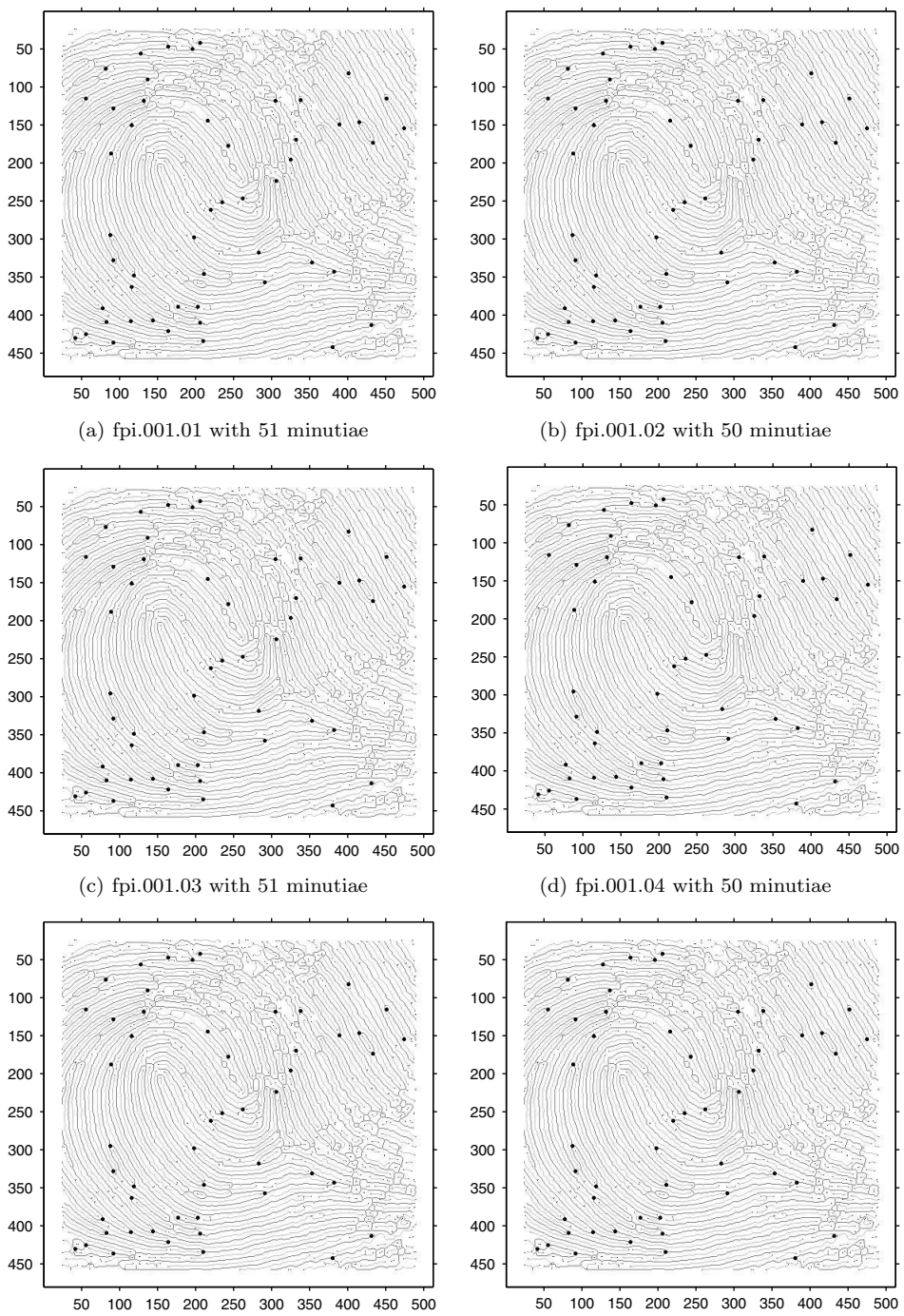

(a) fpi.001.01 with 51 minutiae

(b) fpi.001.02 with 50 minutiae

(c) fpi.001.03 with 51 minutiae

(d) fpi.001.04 with 50 minutiae

(e) fpi.001.05 with 51 minutiae

(f) fpi.001.06 with 51 minutiae

Fig. 15. Minutiae with scores for different set of noise parameters.

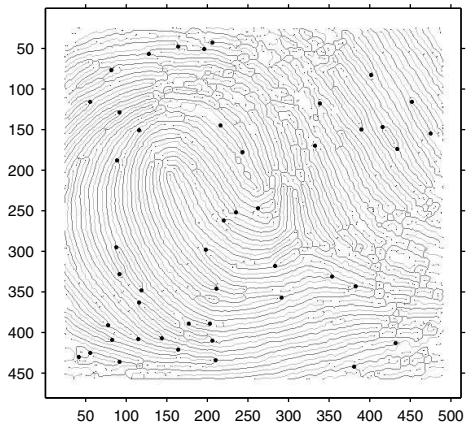

(g) fpi.001.07 with 46 minutiae

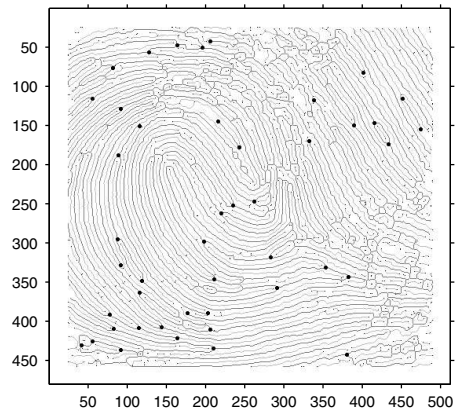

(h) fpi.001.08 with 45 minutiae

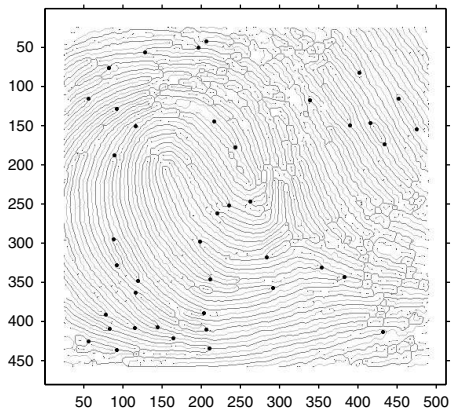

(i) fpi.001.09 with 41 minutiae

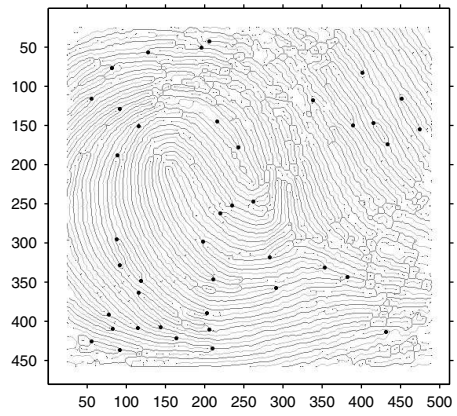

(j) fpi.001.10 with 41 minutiae

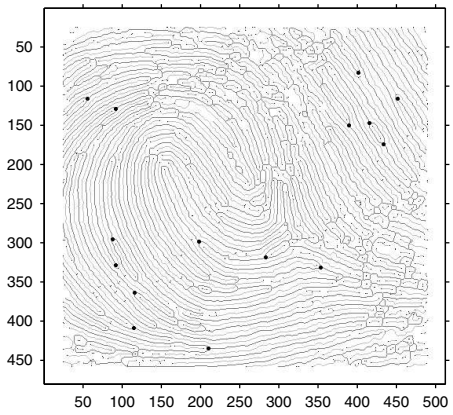

(k) fpi.001.11 with 15 minutiae

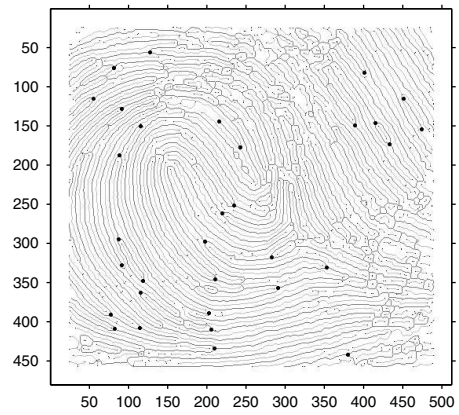

(l) fpi.001.12 with 32 minutiae

Fig. 15. (*Continued*)

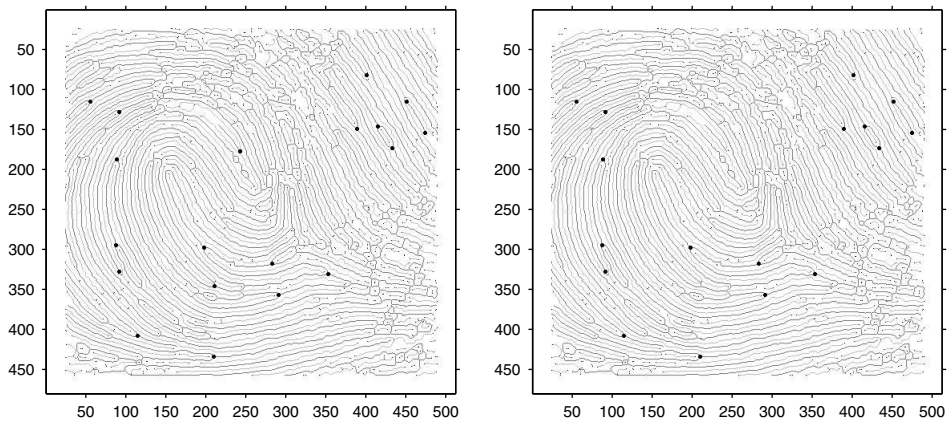

(m) fpi.001.13 with 19 minutiae (n) fpi.001.14 with 17 minutiae

Fig. 15. (*Continued*)

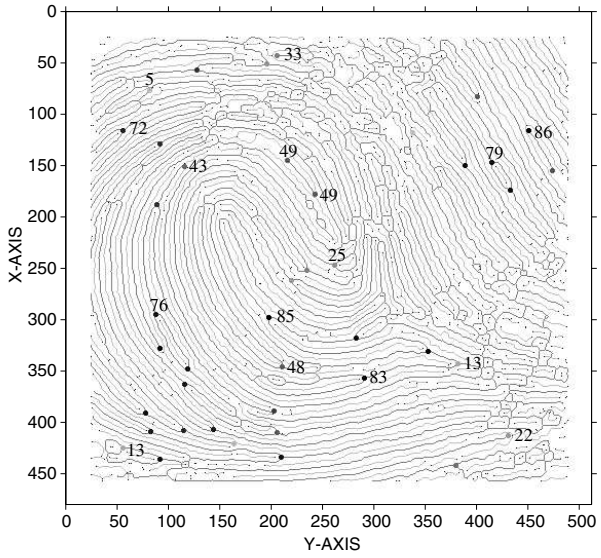

Fig. 16. Minutiae shown with darkness proportional to scores.

and hence, it may not be possible to ascertain which one of them appears before bifurcation and which two are the bifurcated ridges. Hence, it is hard to calculate the local ridge angle at P_1 that is required as a guiding direction to find the valley termination minutia expected to be lying between the two bifurcated ridges. This makes the second score component, s_{va}, zero at P_1. Since $s_{ri} + s_{va} = 0$, it is not meaningful to find the negative score imparted by noise, and therefore, by default,

s_{no} becomes zero. Thus, the total score of minutia P_1 becomes 0, and it is not shown in Figs. 15(a)–15(n) and Fig. 16.

In the next minutiae P_2 (type: Bifurcation, x: 345, y: 210) of Fig. 17, the first component of score, s_{ri}, due to ridge topographical structure in and around P_2, is 34. But the valley termination minutia, supposed to be present near P_3 and within the two bifurcated ridges, is not present. Instead, the said valley termination minutia is lying outside the two bifurcated ridges. To measure the distances $d_{pp'}$, $d_{p''r_1}$, $d_{p''r_2}$, $d_{p''v_1}$, and $d_{p''v_2}$ in the set $\{d_{BM,va}\}$, the said valley termination minutia is the basic pre-requisite. So the score component due to valley topography, s_{va}, for P_2 is as low as 14. The noise level, η, in the window centered at P_2, falls short of the threshold noise, τ_{noise}, set for our chosen set of parameters, and therfore, s_{no} for P_2 turns to be zero. The total score of P_2 thus amounts to be $34 + 14 - 0 = 48$.

In the minutiae P_3 (type: Bifurcation, x: 424, y: 55), s_{ri} is found to be 35. This minutia has narrowly escaped to be marked as a loop minutia, since we have set that

Table 4. (a) Score values of bifurcation minutiae.

No.	x	y	Angle	Score
1	76	81	315	5
2	342	381	267	13
3	424	55	267	13
4	261	219	41	21
5	50	195	258	24
6	246	261	71	25
7	251	234	248	32
8	441	379	93	38
9	409	205	252	47
10	345	210	250	48
11	56	127	91	65
12	187	88	328	65
13	128	91	304	66
14	407	114	251	67
15	115	55	305	72
16	408	82	246	74
17	362	115	40	75
18	406	143	252	75
19	294	87	14	76
20	173	432	215	77
21	347	118	229	78
22	433	209	270	78
23	390	77	235	78
24	435	91	267	79
25	146	414	23	79
26	149	388	217	80
27	317	282	108	82
28	356	290	286	83
29	330	352	254	84
30	297	197	39	85

Table 4. (b) Score values of termination minutiae.

No.	x	y	Angle	Score
1	117	337	222	6
2	420	163	75	9
3	412	430	114	22
4	42	205	270	33
5	150	115	116	43
6	82	400	41	47
7	144	215	223	49
8	177	242	34	49
9	154	473	15	50
10	388	202	90	60
11	327	91	22	82
12	115	450	216	86

each of the edge lengths of a loop should be less than 2λ. The valley termination minutia is found to be present near P_3 between the two bifurcated ridges. Distances in set $\{d_{BM,va}\}$ are measured, and s_{va} is found to be 39. However, it is evident from the figure that this minutia is located in a highly noisy area, and the score component s_{no} is found to be -61 as expected. The total score of P_3 thus becomes $35 + 39 - 61 = 13$.

In the fourth minutia P_4 (type: Bifurcation, x: 297, y: 197), s_{ri} and s_{va} are estimated to be 37 and 48 respectively, whereas, s_{no} is zero. Total score of P_4 thereby amounts to $37 + 48 - 0 = 85$. The topographic orderliness of the local neighborhood of P_4 clearly supports the authenticity of the score yielded by the procedure followed.

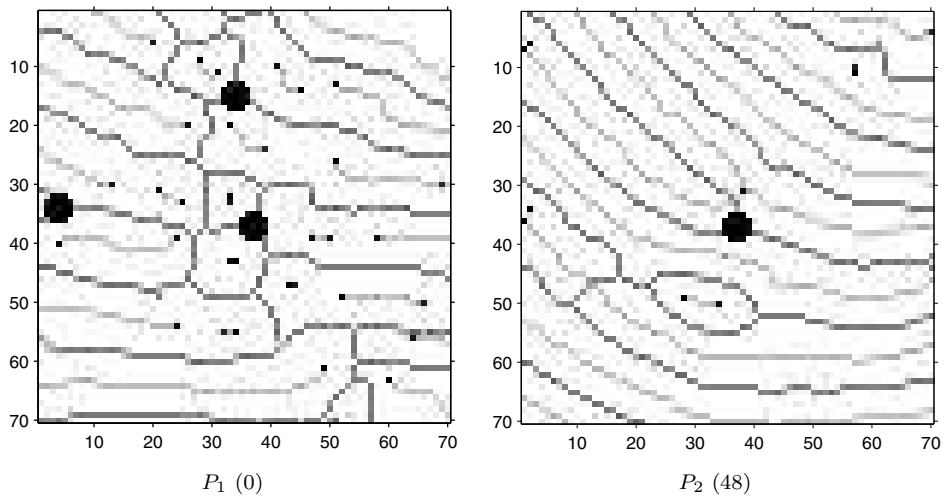

Fig. 17. Minutiae $\{P_1, P_2, P_3, P_4\}$ of image fpi.001 in their local neighborhood.

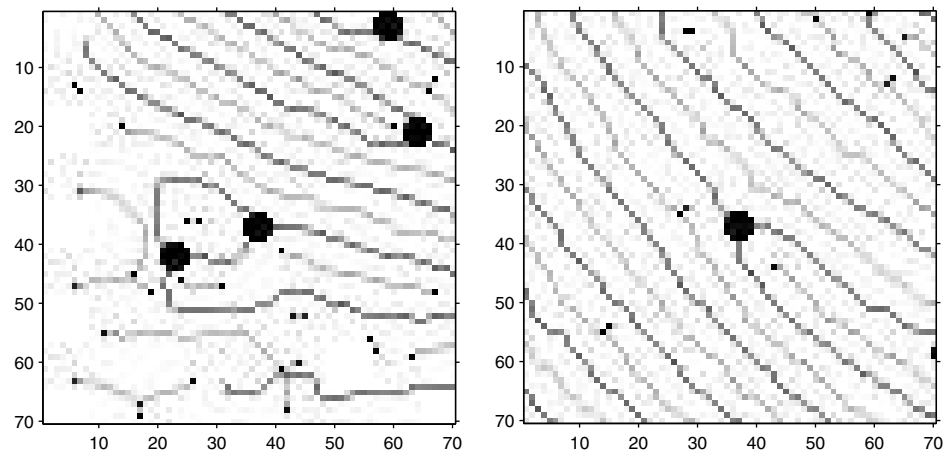

Fig. 17. (*Continued*)

The proposed method is implemented in C on a Sun_Ultra 5_10, Sparc, 233 MHz, the OS being the SunOS Release 5.7 Generic. The total CPU time for the evaluation of scores of all minutiae in a ternary skeletonized fingerprint image was found to be around 0.03 to 0.07 sec.

6. Conclusion and Future Works

This work elucidates a mechanism for assigning a score value to each of the extracted minutiae, based on its topographical properties. Further improvements could be achieved by designing an appropriate strategy for cross-checking the prominence of a minutia in the original gray-scale image and the smoothness of curvature of the ridge lines and valley lines in its local neighborhood in the ternary skeletonized image.

The score values obtained for a set of minutiae can be used to expedite a fingerprint matching process. A future research problem would be to devise a hierarchial arrangement of the minutiae based on the minutiae scores in order to reduce the time for an unsuccessful match. Searching for a fingerprint match in a fingerprint database containing millions of records may take an inordinate amount of time that can be reduced significantly by adopting a suitable cascading technique on the minutiae hierarchy. Fingerprint indexing by Bhanu and Tan[2] strengthens our assertion on minutiae scores for faster fingerprint recognition.

A complete AFIS is currently being developed by us based on minutiae matching with scores assigned to them. The aforesaid matching module takes into consideration the score values of the minutiae to speed up a fingerprint matching process[3] using an efficient technique based on a new point-set pattern matching algorthim.[4] The composite module will be available shortly. Experimental evidence in support

of the affirmative role of minutiae scores on fingerprint matching techniques will be reported in a future paper.

References

1. American National Standards Institute, *Fingerprint Identification — Data Format for Information Interchange*, New York (1986).
2. B. Bhanu and X. Tan, "Fingerprint indexing based on novel features of minutiae triplets," *IEEE Trans. on Pattern Analysis and Machine Intelligence* **25**(5), 616–622 (2003).
3. P. Bhowmick, A. Bishnu, B. B. Bhattacharya, M. K. Kundu, C. A. Murthy and T. Acharya, "Determination of minutiae scores for fingerprint image applications," *Proc. 3rd Indian Conference on Computer Vision, Graphics and Image Processing*, pp. 463–468 (2002).
4. A. Bishnu, S. Das, S. C. Nandy and B. B. Bhattacharya, "An improved algorithm for point set pattern matching under rigid motion," *Proc. 5th Italian Conference on Algorithms and Complexity, CIAC 2003, LNCS* **2653**, 36–45.
5. G. T. Candela, P. J. Grother, C. I. Watson, R. A. Wilkinson and C. L. Wilson, *PCASYS — A Pattern-Level Classification Automation System for Fingerprints*, NISTIR 5647, National Institute of Standards and Technology (August 1995).
6. A. Ceguerra and I. Koprinska, "Integrating local and global features in automatic fingerprint verification," *16th Int. Conference on Pattern Recognition* **3**, 347–350, (2002).
7. A. Farina, Zs. M. Kovács-Vajna and A. Leone, "Fingerprint minutiae extraction from skeletonized binary images," *Pattern Recognition* **32**, 877–889 (1999).
8. Fingerprint Verification Competition (2000), http://bias.csr.unibo.it/fvc2000/download.asp.
9. F. Galton, *Fingerprints*, London, Macmillan (1892).
10. R. Haralick, "Ridges and valleys on digital images," *Comput. Vis. Graph. Imag. Process.* **22**, 28–38 (1983).
11. Y. He, J. Tian, X. Luo and T. Zhang, "Image enhancement and minutiae matching in fingerprint verification," *Pattern Recognition Letters* **24**(9–10), 1359–1370 (June 2003), (to appear).
12. A. K. Hrechak and J. McHugh, "Automated fingerprint recognition using structural matching," *Pattern Recognition* **23**, 893–904 (1990).
13. D. C. D. Hung, "Enhancement and feature purification of fingerprint images," *Pattern Recognition* **26**, 1661–1671 (1993).
14. A. Jain, L. Hong and R. Bolle, "On-line fingerprint verification," *IEEE Trans. on Pattern Analysis and Machine Intelligence* **19**, 302–313 (1997).
15. A. K. Jain, S. Prabhakar, L. Hong and S. Pankanti, "Filterbank-based fingerprint matching," *IEEE Trans. on Image Processing* **9**, 846–859 (2000).
16. X. Jiang and W. Ser, "Online fingerprint template improvement," *IEEE Trans. on Pattern Analysis and Machine Int.* **24**(8), 1121–1126 (2002).
17. Zs. M. Kovács-Vajna, "A fingerprint verification system based on triangular matching and dynamic time warping," *IEEE Trans. on Pattern Analysis and Machine Intelligence* **22**, 1266–1276 (2000).
18. Zs. M. Kovaćs-Vajna, R. Rovatti and M. Frazzoni, "Fingerprint ridge distance computation methodologies," *Pattern Recognition* **33**, 69–80 (2000).
19. C. H. Lin, J. H. Liu, J. W. Ostenburg and J. D. Nicol, "Fingerprint comparison. I: similarity of fingerprints," *Journal of Forensic Sciences* **27**, 290–304 (1982).

20. D. Maio and D. Maltoni, "Direct gray-scale minutiae detection in fingerprints," *IEEE Trans. on Pattern Analysis and Machine Intelligence* **19**, 27–39 (1997).
21. B. M. Mehtre and N. N. Murthy, "A minutia based fingerprint identification system," *Proceedings Second International Conference on Advances in Pattern Recognition and Digital Techniques*, Calcutta (1986).
22. B. M. Mehtre, N. N. Murthy, S. Kapoor and B. Chatterjee, "Segmentation of fingerprint images using directional image," *Pattern Recognition* **20**, 429–435 (1987).
23. *MINUBIN: Minutiae Extraction from a Skeletonized Binary Fingerprint Image*, Technical Report No. ACMU/INTEL/2002/1, 2002, Advanced Computing and Microelectronics Unit, Indian Statistical Institute, Kolkata, India.
24. L. O'Gorman and J. V. Nickerson, "An approach to fingerprint filter design," *Pattern Recognition* **22**, 29–38 (1989).
25. F. Pernus, S. Kovacic and L. Gyergyek, "Minutiae-based fingerprint recognition," *Proc. 5th International Conference on Pattern Recognition*, pp. 1380–1382 (1980).
26. S. Prabhakar, A. K. Jain and S. Pankanti, "Learning fingerprint minutiae location and type," *Pattern Recognition* **36**(8), 1847–1857 (2003).
27. C. I. Watson and C. L. Wilson, *Fingerprint Database*, National Institute of Standards and Technology, Special Database 4, FPDB, (April 1992).
28. N. Ratha, S. Chen and A. K. Jain, "Adaptive flow orientation based feature extraction in fingerprint images," *Pattern Recognition* **28**, 1657–1672 (1995).
29. *RIVEX: Extraction of Ridge and Valley Skeletons from a Gray-scale Fingerprint Image*, Technical Report No. ACMU/INTEL/2002/2, 2002, Advanced Computing and Microelectronics Unit, Indian Statistical Institute, Kolkata, India.
30. W. Shu, G. Rong, Z. Bian and D. Zhang, "Automatic palmprint verification," *International Journal of Image and Graphics* **1**(4), 135–151 (2001).
31. J. H. Wegstein, *An Automated Fingerprint Identification System*, US Government Publication, Washington (1982).
32. A. J. Willis and L. Myers, "A cost-effective fingerprint recognition system for use with low-quality prints and damaged fingertips," *Pattern Recognition* **34**, 255–270 (2001).

Appendix

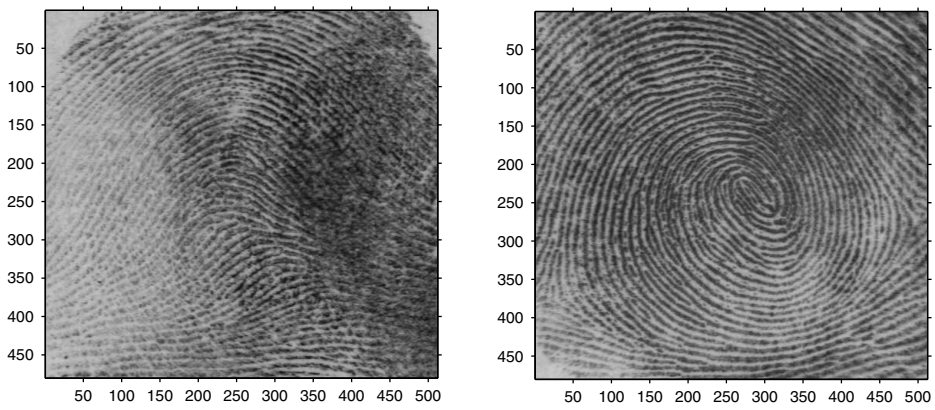

Fig. 18. Sample gray-scale images from NIST sdb-4.

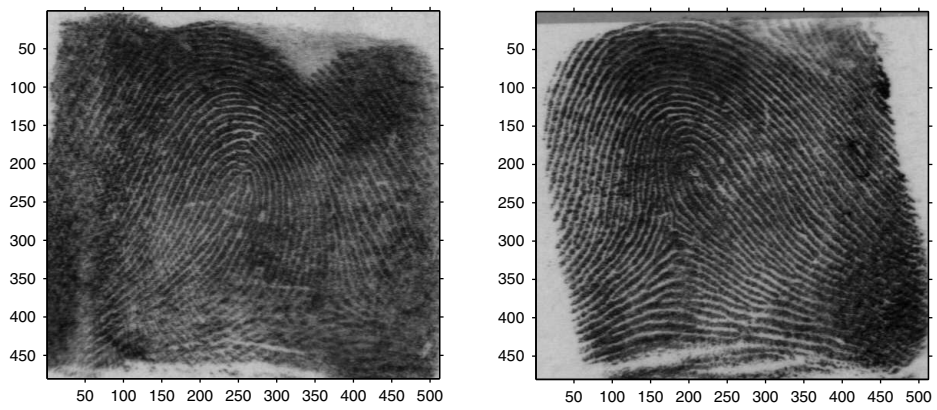

(c) (d)

Fig. 18. (*Continued*)

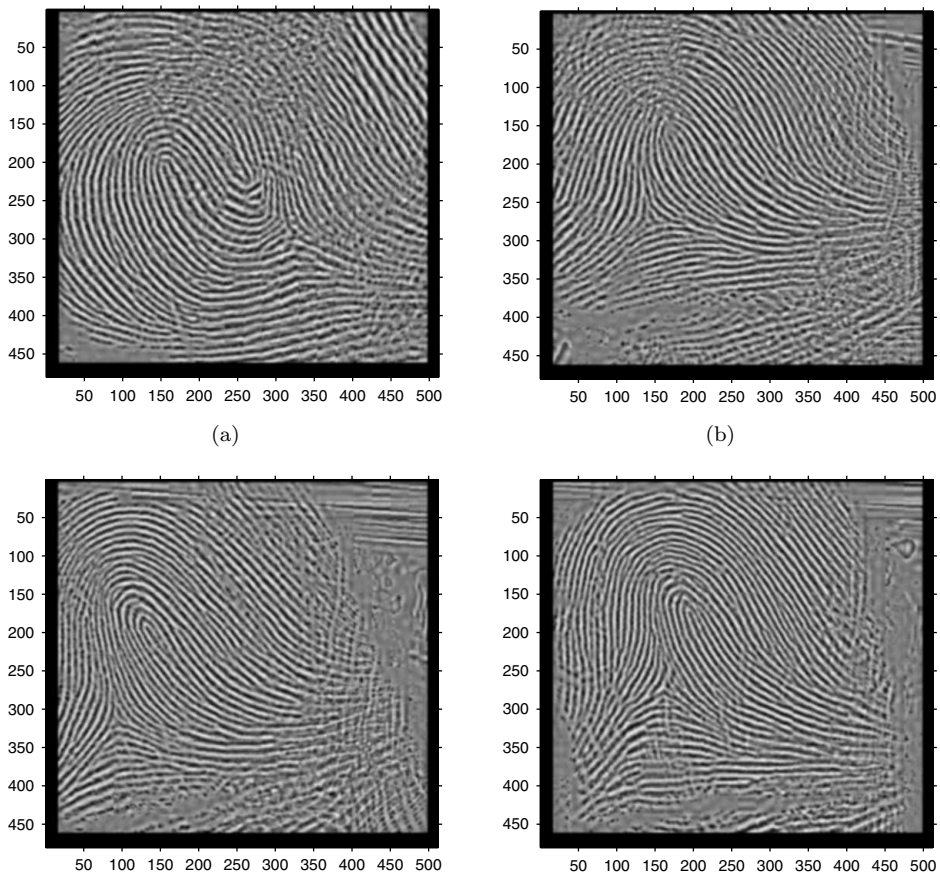

(a) (b)

(c) (d)

Fig. 19. Sample gray-scale images from NIST sdb-14.

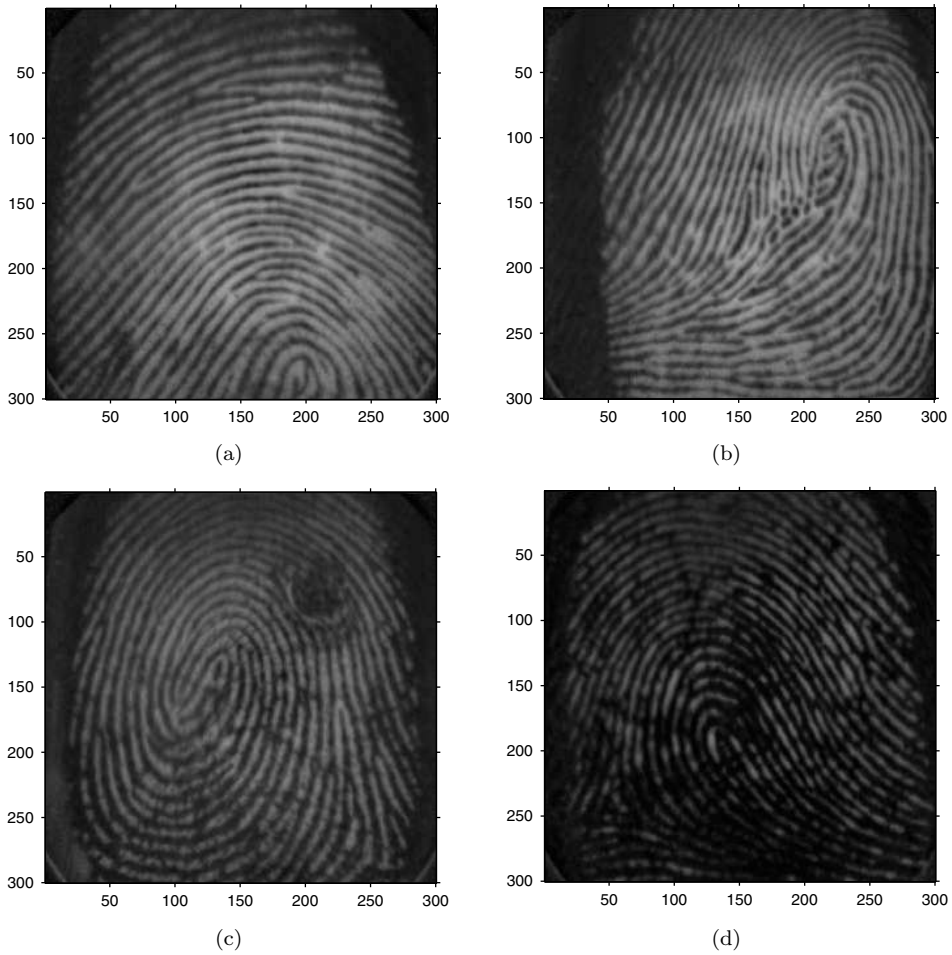

Fig. 20. Sample gray-scale images from FVC-2000 sdb-B1.

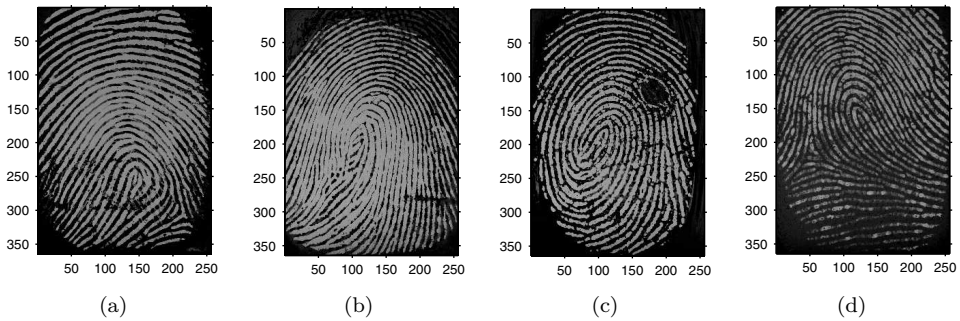

Fig. 21. Sample gray-scale images from FVC-2000 sdb-B2.

Partha Bhowmick received the B.Tech. (Hons.) degree in manufacturing science and engineering (mechanical) from the Indian Institute of Technology, Kharagpur, India, and Master of Technology in computer science from the Indian Statistical Institute, Kolkata, India. Currently, he is in the Faculty of Bengal Engineering College (DU), Howrah, India. His research interest includes algorithms and image processing.

Arijit Bishnu received his BE degree in electrical engineering from R.E.C., Durgapur, India in 1995. He received the Master of Technology in computer science and PhD degrees from the Indian Statistical Institute, Kolkata, India in 1998 and 2003 respectively. Currently he is an Associate in the School of Information Sciences, Japan Advanced Institute of Science and Technology, Japan. His research interest includes algorithms and image processing.

Bhargab B. Bhattacharya received the BSc degree in physics from the Presidency College, Calcutta, the B.Tech. and M.Tech. degrees in radiophysics and electronics, and the PhD degree in computer science all from the University of Calcutta, India. Since 1982, he has been in the faculty of the Indian Statistical Institute, Calcutta, where he is a professor. He visited the Department of Computer Science and Engineering, University of Nebraska-Lincoln, USA, during 1985–1987, and again in 2001–2002, and the Fault-Tolerant Computing Group, Institute of Informatics, at the University of Potsdam, Germany during 1998–2000. His research interest includes logic synthesis and testing of VLSI circuits, physical design, graph algorithms, and image processing architecture. He has published more than 120 papers in archival journals and refereed conference proceedings, and filed 7 United States Patents (pending). Currently, he is collaborating with Intel Corporation, USA, and IRISA, France, for the development of image processing hardware and reconfigurable parallel computing tools.

Dr. Bhattacharya is a Fellow of the Indian National Academy of Engineering. He served on the conference committees of the International Test Conference (ITC), the Asian Test Symposium (ATS), the VLSI Design and Test Workshop (VDAT), the International Conference on Advanced Computing (ADCOMP), and the International Conference on High-Performance Computing (HiPC). For the International Conference on VLSI Design, he served as the Tutorial Co-Chair (1994), Program Co-Chair (1997), General Co-Chair (2000), and as a member of the Steering Committee since 2001. He is on the editorial board for the Journal of Circuits, Systems,

and Computers (World Scientific, Singapore), and the Journal of Electronic Testing: Theory and Applications (JETTA).

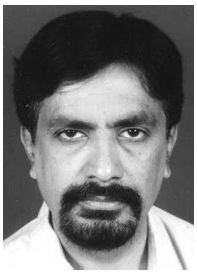

Malay K. Kundu received his B.Tech., M.Tech. and PhD (Tech.) degrees in Radio physics and Electronics from the University of Calcutta. In 1982, he joined the Indian Statistical Institute, Calcutta, as a faculty member. He had been the Head of the Machine Intelligence Unit of the Institute from September 1993 to November 1995 and currently he is a full professor of the same unit. His current research interest includes image processing and analysis, image compression, digital watermarking, wavelets, fractals, VLSI design for digital imaging and soft computing.

He received the prestigious VASVIK award for industrial research in Electronic Sciences and Technology for the year 1999 and the Sir J. C. Bose memorial award in 1986. He has contributed about 75 research papers in well known and prestigious archival journals, international refereed conferences and as chapters in monographs and edited volumes. He is co-author of the book titled *Soft Computing for Image Processing* published from Physica-Verlag, Heidelberg. He is a Fellow of the National Academy of Sciences, India and the Institute of Electronics and Telecommunication Engineers, India.

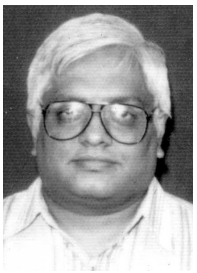

C. A. Murthy received the B.Stat (Hons), M.Stat., and PhD degrees from the Indian Statistical Institute (ISI), Kolkata. He visited the Michigan State University, East Lansing in 1991–1992 for six months, and the Pennsylvania State University, University Park during 1996–1997. He is a professor in the Machine Intelligence Unit of ISI. His fields of research interest include pattern recognition, image processing, machine learning, neural networks, fractals, genetic algorithms, wavelets and data mining. He received the best paper award in 1996 in Computer Science from the Institute of Engineers, India. He received the Vasvik award for Electronic Sciences and Technology for 1999 along with his two colleagues. He is a Fellow of the Indian National Academy of Engineering.

Dr. Tinku Acharya is a Senior Executive Vice President and the Chief Science Officer of Avisere Inc., Tucson, Arizona, USA. He is also an Adjunct Professor in the Department of Electrical Engineering, Arizona State University, Tempe, Arizona. He received his BSc (Honors) in Physics, B.Tech. and M.Tech. in Computer Science from the University of Calcutta, India and his PhD in Computer Science from the University of Central Florida, Orlando, Florida.

Dr. Acharya held many leading positions in Intel Corporation, Arizona (1996, 2002), AT&T Bell Laboratories (1995–1996), Institute of Systems Research, University of Maryland at College Park (1994–1995), National Informatics Center, Government of India (1988–1990), and held visiting faculty positions at Indian Institute of Technology (IIT), Kharagpur. He collaborated in research and development with Palo Alto Research Center (PARC) of Xerox Corporation, Kodak Corporation, and many other academic institutions and research laboratories worldwide. Dr. Acharya is inventor of 56 awarded US patents and 7 European Patents. He was recognized as the Most Prolific Inventor in Intel Corporation Worldwide in 1999 and consecutive five years (1997–2001) in Intel Arizona. He contributed more than 60 referred technical papers published in International Journals, conferences, and book chapters. He is co-author of the book *Data Mining: Multimedia, Soft Computing and Bioinformatics*, John Wiley & Sons, Inc., New Jersey.

Dr. Acharya is a Fellow of IETE, Senior Member of IEEE, SPIE Optical Society. He served in the US National Body of JPEG2000 Standard committee (1998–2002). His current research interests are in computer vision, multimedia computing, biometrics, multimedia data mining, VLSI architectures and algorithms.